In an effort to determine the quantum efficiency of the HRC detectors throughout the range of energies at which AXAF is expected to operate, two test detectors with near-identical MCPs to the HRC flight plates were taken to the Synchrotron Radiation Source (SRS) facility at Daresbury (UK). The measurement of quantum efficiency features relating to absorption edges of the photocathode (and the underlying lead silicate glass) was of particular interest, especially in terms of the HRC-S detectors where instrument features must not be confused with line features from astrophysical sources. We here describe the efficiency measurements of two plates installed on beamline 1.1 (450 eV to 1200 eV) and beamline 4.2 (4.5 keV to 9.5 keV) in October 1997.

1 QUANTUM EFFICIENCY MEASUREMENTS

The two stage 'chevron' test detectors comprised Philips Photonics low noise glass MCPs,[?] 36 mm in diameter with a microchannel bias angle of 6°. Channel diameter and pitch were 12.5 μm and 15 μm respectively, with a length-diameter ratio of 120:1 and nominal 63% open area fraction. The detector was coated on one half of the front plate with ~14000 Å CsI, the other half was left bare for comparison.

Measurements of the MCP detector efficiencies were made during SRS low ring current (~20 μA) operation, providing the reduced X-ray flux necessary to prevent electronic overload and also damage to the front MCP. The $\frac{1}{e}$ lifetime of the beam in this mode was ~50 hours. Previous campaigns at Daresbury[?,?] have led us to realise that the source energy spectrum measured using a charge replacement foil at the time of single (~20 mA) or multi-bunch (~150 mA) operation of the SRS is not a good description of the beam energy profile during low ring current. Therefore, the beam flux was monitored on both beamlines using separate single-wire, gas filled proportional counters (PCs).

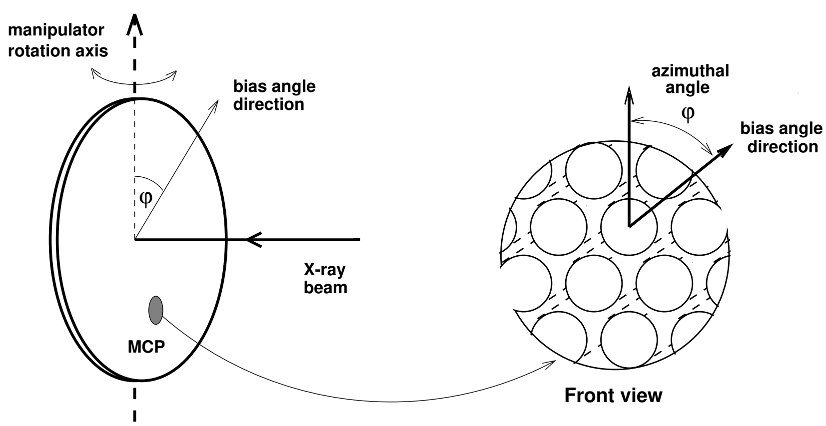

Figure 1: Definition of the azimuth angle ϕ. A *normal incident* beam will have a *channel incidence* of 6° (i.e. equal to the bias angle) regardless of ϕ.

Both MCP detectors were secured on a manipulator capable of linear movement along the two axes orthogonal to the beam, and rotation about a vertical axis. Upon assembly, the front MCP of the 1.1 detector was orientated such that the channel bias direction in the plane of the plate was parallel to the detector rotation axis (i.e. ϕ=0°, see Fig. 1). Thus, a minimum *channel incidence* angle of 6° with respect to the beam occurred with the beam at *normal incidence* to the plate. The front plate of the 4.2 detector however, was rotated by 90° with respect to this (ϕ=90°) such that a minimum channel incidence of 0° could be achieved. Efficiency measurements were made at various beam angles to the front plate normal to simulate the AXAF cone angles of ±1.8° and ±3.4°, due to X-ray reflections off the inner and outer shells of the High Resolution Mirror Assembly (HRMA).

1.1 Beamline 1.1

The beamline optics of 1.1 consist of a horizontally deflecting, water-cooled cylindrical mirror (Pt coated CVD SiC), three interchangeable spherical nickel (Ni) and gold (Au) coated gratings with ion etched rulings of (1) 1050, (2) 1500 and (3) 1800 lines mm^{-1}, and a post-focussing Pt coated spectrosil ellipsoid mirror. Switching between the Ni and Au coated grating sections provides practical flux in the ranges 250 to 850 eV and 700 to 1200 eV respectively. Initial tests showed the Ni(3) and Au(1) gratings to be best suited to our needs[1] with energy resolutions of about 0.5 eV and 1.0 eV respectively.

The gas filled proportional counter (P10 at ~1 bar) was situated some 60 cm up-beam from the MCP detector on a pneumatically operated vertical linear drive. Moving the PC in and out of the beam allowed us to interleave energy scans using either the PC or MCP detector. Initial measurements were necessary to determine the drive position at which the beam was aligned with the PC window.

The polypropylene window on the PC was supported by a 46% transmission mesh and was ~1.0 μm thick. The window was aerosol coated on its interior with a carbon spray to form a conductive layer and prevent localised charging of the polypropylene which would compromise the PC performance. Prior measurements of window transmission on beamline 1.1 showed evidence of oxygen absorption at 534 eV hypothetically due to aerosol solvent OH groups being absorbed into carbon coat during drying. This effect was modelled and included in the window transmission data used during analysis. The absorption efficiency of the P10 gas was calculated as 100% over the beamline 1.1 energy range.

1.1.1 Ni(3) grating, 450 to 800 eV

The proportional counter allowed us to not only measure the low current photon flux but, by recording pulse height distributions (PHDs) at 20 eV energy intervals, determine the spectral purity of the beam. Figure 2 shows four such PHDs recorded from the Ni(3) grating. Substantial second order contamination is obvious at the lower energies. By fitting Gaussian distributions to these PHDs and correcting for PC window transmission we were able to quantify the contamination due to second and third order harmonics (see Fig. 3). Unfortunately, carbon contamination of the Ni(3) grating increased the second and third order dominance of the flux from the C-K edge (284 eV) to about 450 eV. The quality of the PHD fits in this range was poor, therefore data will not be presented within this region. Oxygen contamination of the beamline was also a well known feature and is apparent by the large drop in countrate at 534 eV.

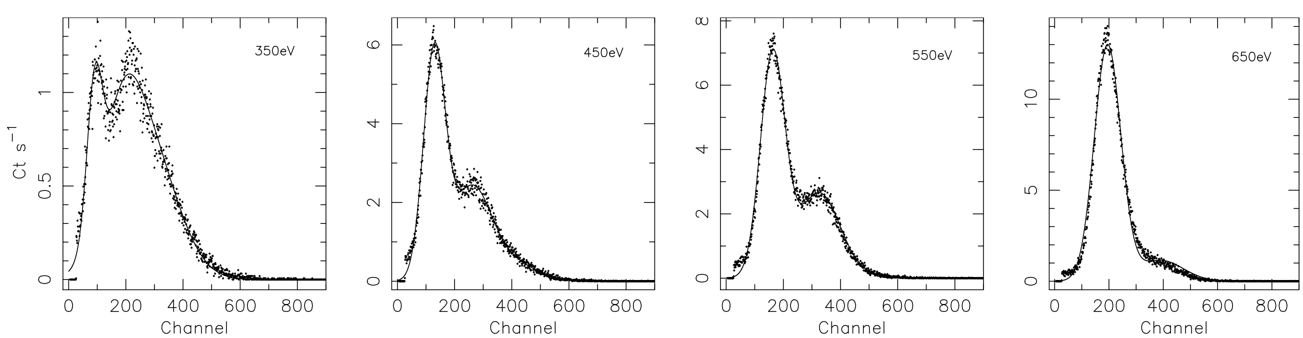

Figure 2: PC pulse height distributions of the Ni(3) grating on beamline 1.1. The solid curve represents three Gaussian fits with second and third order peak positions frozen in association with that of the fitted first peak.

We can represent the incident flux at the MCP detector (I_{MCP}) for any given energy as,

$$I_{\mathrm{MCP}} = T_{\mathrm{mesh}}\,(e_1 I_1 + e_2 I_2 + e_3 I_3) \tag{1}$$

[1]Unfortunately, contamination of the Au(2) and (3) gratings was seen to seriously degrade the spectral purity of the beam flux.

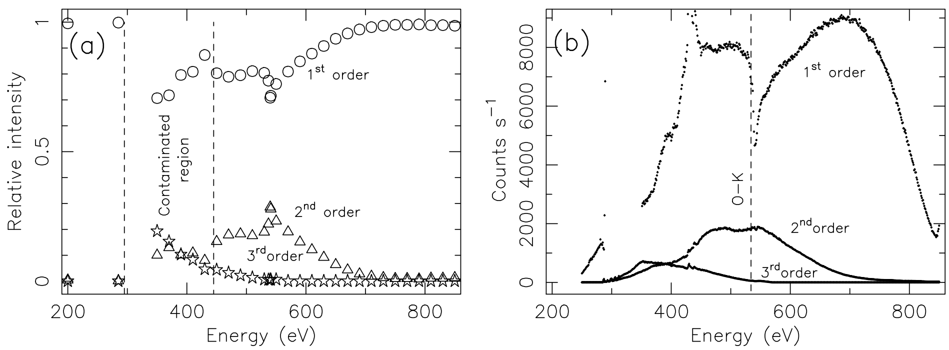

Figure 3: (a) Degree of second and third order contamination of the beamline 1.1 flux from the Ni(3) grating. Data has been corrected for 1.0 μm polypropylene and 46% transmission support mesh on the PC window. (b) Calculated first, second and third order beam flux.

where $e_{1..3}$ are the detector efficiencies and $I_{1..3}$ are the count rates due to the first, second and third orders, respectively. The transmission of a metal mesh in front of the detector MCP (T_{mesh}) was assumed as 0.9 throughout. Previous quantum efficiency measurements of CsI coated MCP detectors[?,?] were used to estimate values for e_2 and e_3, allowing the first order efficiency to be computed.

Figure 4 shows the absolute quantum efficiency of the CsI coated section of the MCP calculated using Eqn. 1 where $I_{1..3}$ are as shown in Fig. 3b. The model shown in Fig. 4 was generated by software initially developed and cited by Fraser[?,?] and is discussed at length by Pearce.[?] The feature at 541 eV has not previously been observed and is most likely a complication due to the oxygen contamination of the beamline and PC window. Of particular interest is the slow onset of the I and Cs-$M_{\mathrm{iv\text{-}v}}$ edges shown in Fig. 4b & c. This effect, previously observed at the SRS using an identical MCP detector,[?] and in the photocurrent and reflectivity measurements of several high-Z metals,[?,?] is primarily a characteristic of the 3d→f atomic transition.[?]

1.1.2 Au(1) grating, 700 to 1200 eV

Proportional counter PHDs of the beam from the Au(1) grating were recorded in 20 eV energy steps as before, and confirmed that the flux was free from second and third order harmonics. After switching gratings the beam position was checked using the MCP imaging electronics as movement would require re-alignment of the PC. Initial checks suggested that the beam had not significantly moved with respect to the MCP. Unfortunately, post-analysis indicated that the flux had moved within the bounds of the beam spot, to the very edge of the PC window[2] resulting in some loss of counts (see Fig.5) and an artificially high MCP efficiency. A single multiplication factor was therefore applied to all the data such that the normal incidence (0°) efficiency curve at 930 eV corresponded to the laboratory derived value at Cu-L. As before, the data was corrected for a carbon coated 1.0 μm polypropylene window and the transmission of the support mesh.

Figure 6 shows the measured quantum efficiency at angles of 0°, 1.8°, 3.4° and 6.4° to the normal incidence of the MCP. The curves shows good consistency with the modelled data and the 930 eV efficiency values at 1.8° and 3.4° closely match the data from the laboratory. The high resolution scans across the Cs $M_{\mathrm{iv\text{-}v}}$ edges (see Fig. 7) exhibit the ~20 eV shift observed using the Ni(3) grating with very similar quantum efficiencies. Evidence of white lines and EXAFS are more prominent at the higher incident angles, an effect previously observed by Pearce.[?] High resolution scans across the I M_{ii} edge at 931 eV (not shown) revealed no significant structure.

[2] an effect made worse since the beam focus was at the front channel plate and not at the PC window further up-beam.

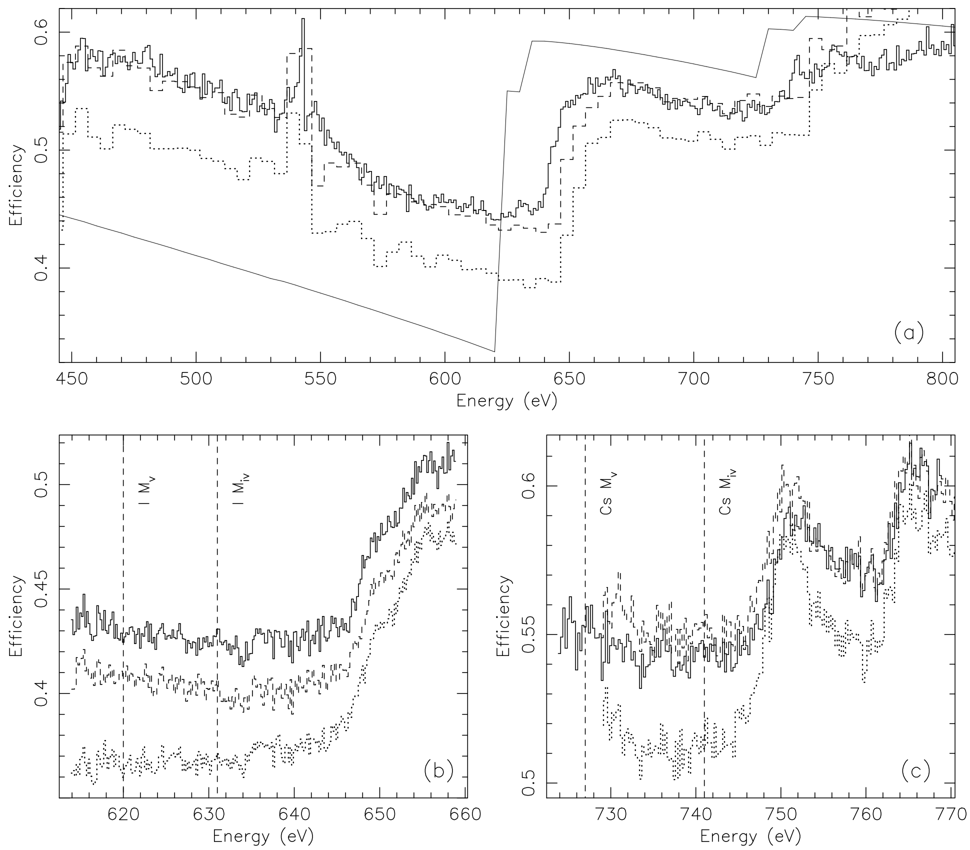

Figure 4: Absolute quantum efficiencies of the CsI coated section of the MCP detector measured on beamline 1.1 using the Ni(3) transmission grating. Beam angles with respect to detector normal incidence are 0° (solid), 1.8° (dashed) and 3.4° (dotted). Solid curve represents modelled data for 0° normal incidence. High resolution scans across the I (b) and Cs (c) $M_{iv\text{-}v}$ edges are in energy steps of 0.2 eV and 0.25 eV respectively.

1.1.3 Analysis

Figure 8 shows the combined efficiency curves from the Ni(3) and Au(1) gratings. The data shows good consistency in the overlapping energy range (700 to 800 eV) and the 'delays' in the Cs $M_{iv\text{-}v}$ edges repeat well. There is also reasonable agreement with the modelled efficiency. None of the $M_{i\text{-}ii}$ edges are seen with any significance.

Figure 9 illustrates the quantum efficiency of the uncoated (bare glass) region of the MCP measured on beamline 1.1 using the Ni(3) and Au(1) gratings. The Ni(3) data has been corrected for second and third order contamination as described previously. The data shows good consistency with the models (given that the specification of the MCP bias angle[?] is 6°±1°) and reemphasises the efficiency gains made by using a CsI photocathode. The most significant feature is the O-K (543 eV) absorption edge where a white line and significant EXAFS are seen. Other structures associated with the contaminates of the lead glass can also be seen and have been previously observed at other energies.[?] The feature at ∼745 eV is possibly the late onset of the Cs M_{iv} edge due to a slight contamination of CsI on the masked side of the MCP during coating.

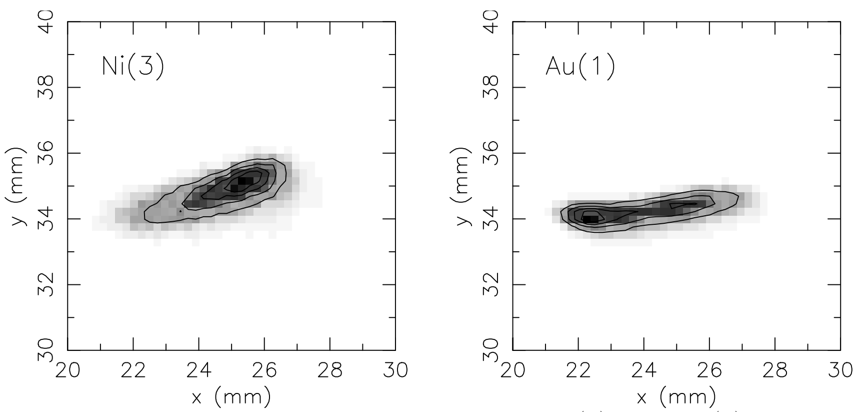

Figure 5: MCP detector images of the beam spot from the Ni(3) and Au(1) gratings at 600 eV and 850 eV, respectively. Contours are at 0.2, 0.4, 0.6 and 0.8 fractions of the peak height.

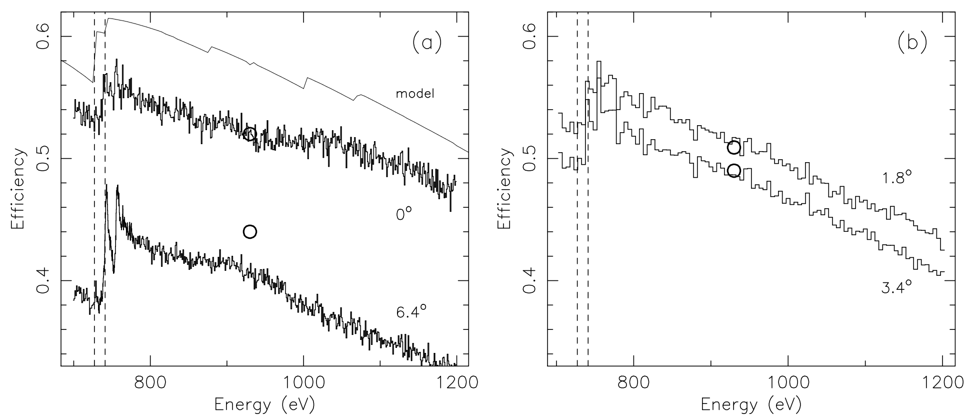

Figure 6: Absolute quantum efficiencies of the CsI coated section of the MCP detector measured on beamline 1.1 using the Au(1) transmission grating. Beam angles are with respect to detector normal incidence. Circles indicate quantum efficiency measurements at Cu-L (930 eV) recorded in the laboratory at Leicester University. Dashed lines are at 727 eV and 741 eV (Cs $M_{v,iv}$ edges, respectively).

1.2 Beamline 4.2

The beamline optics of 4.2 consists of a primary and secondary pre-mirror coated with platinum and chromium respectively, and a silicon (311) double crystal monochromator[?] providing a useable flux in the range 4500 to 9500 eV. The narrow rocking curve associated with these crystals made it necessary to modify the station software such that the feedback to the rocking electronics came from the MCP detector.

Beam reference was provided by a beryllium bodied gas filled (97% Xe, 3% CO_2 at 1.2 bar) single wire proportional counter positioned in the beam behind the MCP detector. The body of the PC was 254 μm thick with an internal diameter of 2.34 cm. PC reference scans were interleaved with MCP measurements by driving the MCP detector in and out of the beam. The transmission of the PC body and the efficiency of the gas were modelled and extracted from the data during analysis.

As previously discussed (Sect. 1), the MCP detector was fixed to a linear drive such that it could be rotated about the vertical axis with a front plate azimuth angle of 90°. Efficiency measurements were made at various beam angles to the front plate microchannel walls to again simulate the AXAF cone angles.

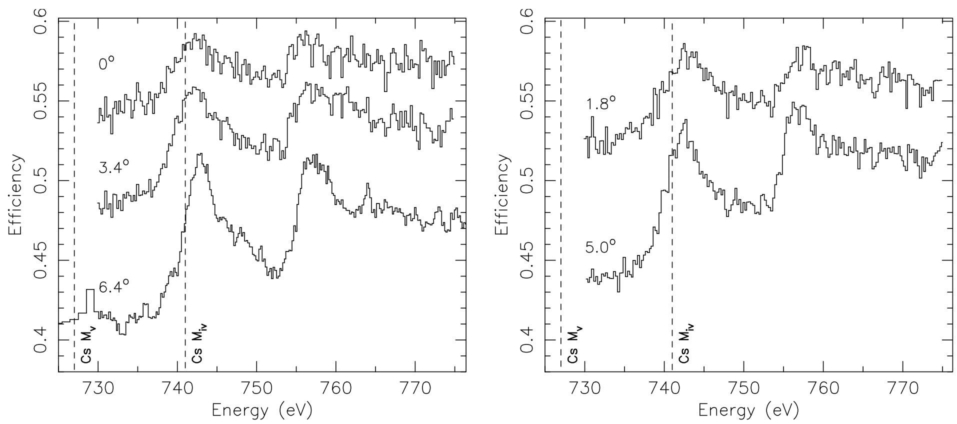

Figure 7: High resolution scans across the Cs $M_{iv\text{-}v}$ absorption edges using the Au(1) grating.

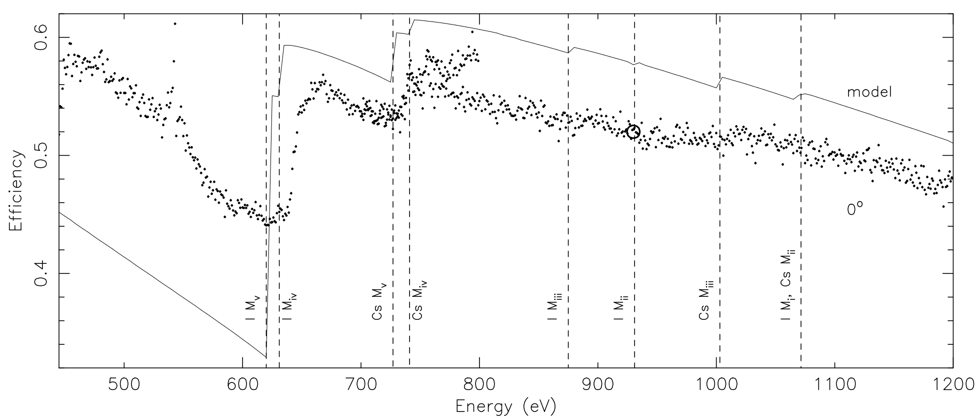

Figure 8: The absolute quantum efficiency of the CsI coated MCP detector at 0° beam incidence measured using the Ni(3) (450 to 800 eV) and Au(1) (700 to 1200 eV) gratings on beamline 1.1. The Leicester laboratory derived efficiency at 930 eV (circle) to which the Au(1) data is normalised is also shown.

1.2.1 Analysis

Unfortunately, during data analysis it was realised that the MCP detector signal wires obscured the beam while recording the PC reference countrate. It was therefore necessary to scale the PC readings to form a continuous curve and normalise the efficiency curves to a previously published value of 12.5% at 5.9 keV for a similar MCP detector.[?] Figure 10a shows the corrected beam intensity as measured using the PC *prior* to removing the gas efficiency and Be window transmission functions (shown in Fig 10b). The feature seen at 5989 eV corresponds to the Cr-K edge due to the coating on the secondary pre-mirror.

Figure 11 shows the measured efficiency of the MCP detector over the full range from 4.5 to 9.5 keV at normal incidence to the CsI coated front plate (i.e. 6° channel incidence). As discussed previously, the data is normalised to 12.5% at 5.9 keV. The data show consistency of form with the both the model and previously published work.[?,?,?] High resolution energy scans across the Cs and I L_{iii} edges were made at various channel incidence angles and are shown in Fig. 12. Strong evidence of white lines is observed across the Cs L_{iii} edge in particular, although it is thought that the features observed at 5042 eV and 5058 eV are due to poor 'rocking' of the monochromator crystals during the period of beam reference measurement.

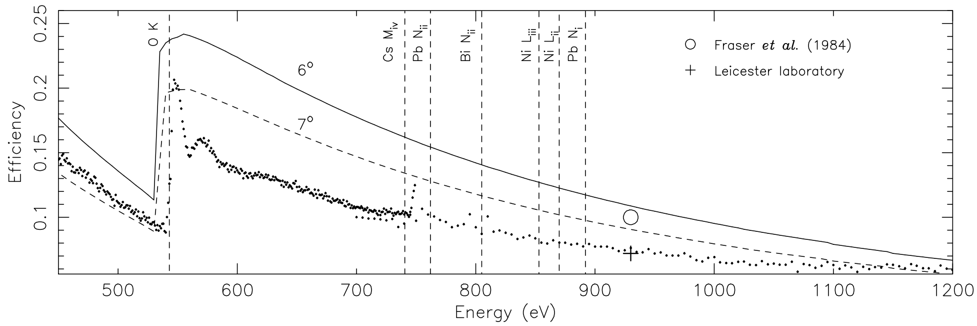

Figure 9: Absolute quantum efficiency of the bare (glass) section of the MCP detector. Solid and dashed lines represent efficiency models for flux at 6° and 7° *channel incidence* respectively. Data is normalised to the Leicester laboratory efficiency value measured at 930 eV (cross).

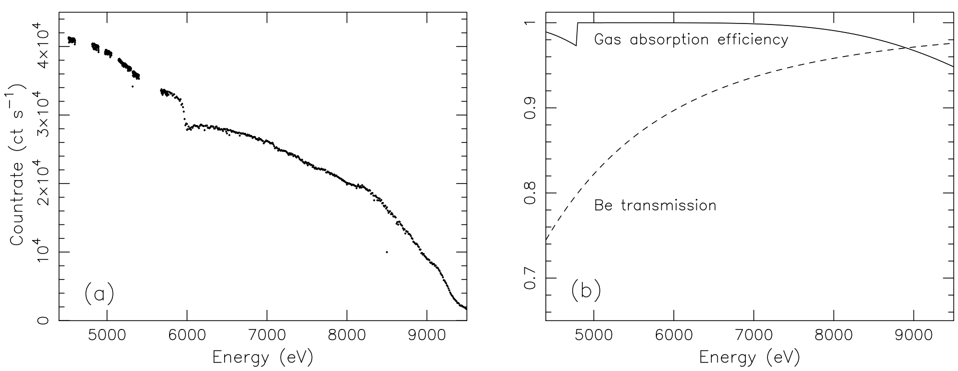

Figure 10: (a) Beamline 4.2 countrate measured using the Be-bodied proportional counter, prior to correcting for (b) the PC gas efficiency and window transmission.

2 Conclusions

This latest (fourth) campaign to the Daresbury SRS has been very successful and provides the most accurate and reliable information regarding the absolute quantum efficiency of the CsI coated MCP detectors of all our campaigns to date.

It is unfortunate however that the spectral contamination of the Ni(3) grating on beamline 1.1 has compromised the quality of the data below ~500 eV although this does emphasise the importance of using the reference proportional counters, both of which performed well. It is also unfortunate that absolute efficiencies could not be calculated from the SRS data alone, however, current improvements in PC design and SRS operating procedures will eliminate the need for data normalisation from future experiments.

The data presented here will be incorporated into the calibration matrix of the Advanced X-ray Astrophysical Facility (AXAF) High Resolution Camera (HRC).

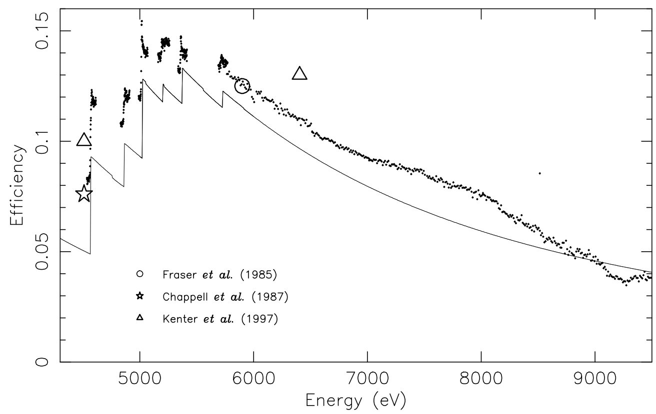

Figure 11: Absolute quantum efficiency of the CsI coated section of the MCP detector at normal incidence to the front plate (6° channel incidence). Solid curve represents the modelled MCP efficiency for 6° channel incidence.

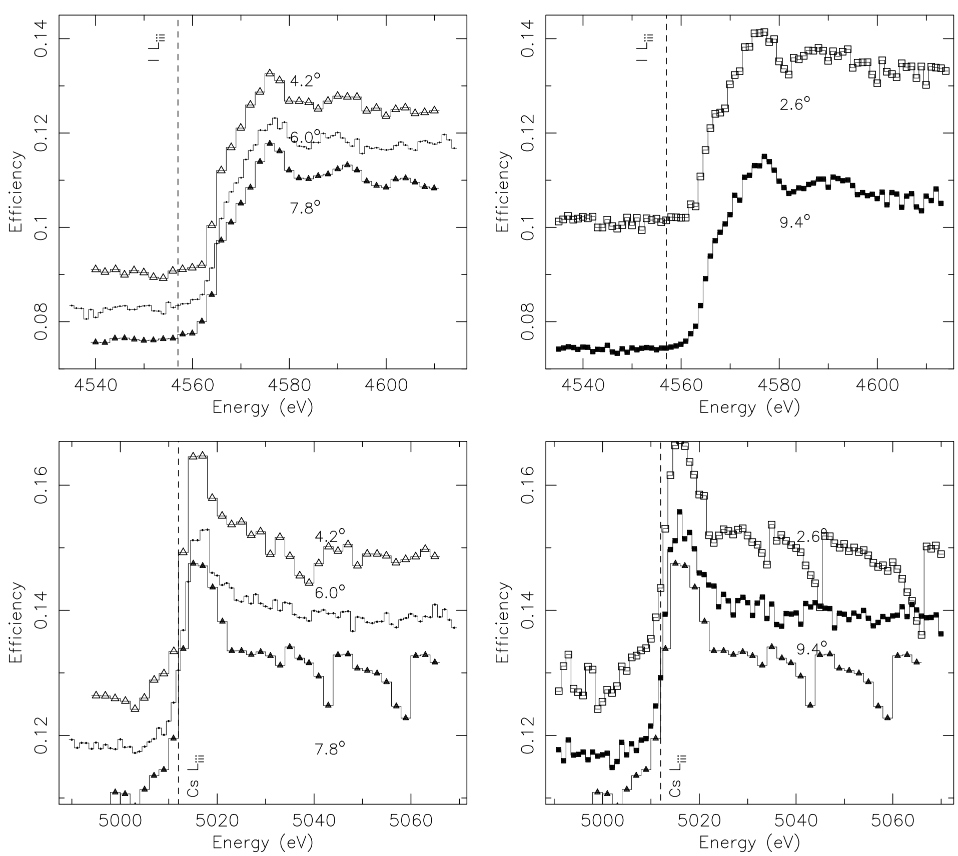

Figure 12: High resolution scans across the I L_{iii} and Cs L_{iii} absorption edges. Beam angles are with respect to the *channel* axis.